Examination of the physical assumptions of a quasi-steady vector model using the integral momentum equation

Wu, C.-H.; Kopp, Gregory

DOI:
10.1016/j.jweia.2019.02.003

Document Version
Peer reviewed version

Citation for published version (Harvard):
Wu, C-H & Kopp, G 2019, 'Examination of the physical assumptions of a quasi-steady vector model using the integral momentum equation', *Journal of Wind Engineering and Industrial Aerodynamics*, vol. 187, 73-84. https://doi.org/10.1016/j.jweia.2019.02.003

Examination of the physical assumptions of a quasi-steady vector model using the integral momentum equation

Chieh-Hsun Wu, Gregory A. Kopp
Boundary Layer Wind Tunnel Laboratory, Faculty of Engineering,
University of Western Ontario, London, ON, Canada N6A 5B9

Correspondence: Gregory A. Kopp
Boundary Layer Wind Tunnel Laboratory, Faculty of Engineering, University of Western Ontario, London, ON, Canada N6A 5B9
Email: gakopp@uwo.ca; Tel: 519-661-2111 ext. 87572; Fax: 519-661-3339

Abstract

Quasi-Steady (QS) vector models have served as a convenient and effective tool for wind load estimations for low-rise buildings in the wind engineering community. In order to understand the applicability for practice, the physical assumptions of a QS vector model are investigated in this paper. The derivation is done through algebraic manipulation of the time-averaged integral momentum equation, which is used to relate mean, area-averaged, roof surface pressures to the mean flow and turbulence field above a roof. The two main assumptions of the QS model are revealed through this process: (i) The streamlines of an instantaneous flow near the roof are assumed to be the mean streamlines so that the instantaneous direction of the flow measured at the reference point is equivalent to the mean direction; (ii) The magnitude of the instantaneous flow is obtained by amplifying the magnitude of the mean flow at a spatially uniform rate such that the amplified magnitude of mean velocity is equivalent to the instantaneous magnitude measured at the reference point. Missing terms in the QS model are used to develop correction terms to improve QS model performance.

Keywords

Quasi-Steady theory; building aerodynamics; wind loads; atmospheric boundary layer; turbulence.

Nomenclature

$A(S_1)$, $A(\mathbf{x}_i)$	Area of the target surface S_1 and i-th tap location, $\boldsymbol{x}_i$, respectively.
Cp	Pressure coefficient.
Cp_{inst}	Instantaneous function associated with the quasi-steady model.
$Cp(S_1)$, $Cp_{\text{inst}}(S_1)$	Spatially averaged pressure coefficient and instantaneous functions, respectively, over surface S_1.
H	Height of the low-rise building model, $H = 8\,\text{cm}$.
I_u	Turbulence intensity of streamwise velocity component.
L_{ux}	Integral length scale of streamwise velocity component.
$\mathbf{n}$	Outward normal of the control volume, i.e., $\mathbf{n} = n_x\mathbf{i} + n_y\mathbf{j} + n_z\mathbf{k}$.
$\mathbf{n}_1$	Outward normal of the target surface portion, S_1, of the control volume.
n	Frequency.
n_s	Sampling rate.
p	Pressure.
p_∞	Ambient static pressure.
S	Bounding surface of the control volume.
S_1	Target surface on roof where area-averaged pressures are calculated.
S_{CpM}, S_{CpQS}	The spectral density of measured and QS-predicted pressures respectively.
$S_{\text{CpQS, CpM}}$	The cross-spectral density between the QS-predicted and measured pressures.
t	Time.
u	Streamwise velocity component (with direction parallel to x-coordinate).
$\mathbf{u}$	Velocity vector, $\mathbf{u} = u\mathbf{i} + v\mathbf{j} + w\mathbf{k}$.
$\mathbf{u}_{\text{m}}$	Velocity measured at point m.
u_H	Upstream streamwise velocity at roof height.
u_{ref}	Reference velocity.
w	Vertical velocity component with direction parallel to z-coordinate.
x	x-coordinate of the space.
$\mathbf{x}$	Space vector, $\mathbf{x} = x\mathbf{i} + y\mathbf{j} + z\mathbf{k}$.
z	Vertical coordinate of the space.
z_o	Roughness length.
θ	Azimuth angle of the wind velocity.
ρ	Density of air.
$\langle a \rangle$, $\overline{a}$	Estimated or (time) averaged value of a.
a'	Temporal fluctuation of a, i.e., $a' = a - \overline{a}$.
$\text{Re}(a)$	Real part of a.

1. Introduction

Understanding the physical mechanisms associated with building surface pressures under the influence of the turbulence in the atmospheric boundary layer (ABL) can greatly help engineers assess risk levels for severe storms. The momentum equations (i.e., the Navier-Stokes equations), which specify the relationship between the velocity and pressure fields, offer a promising tool from the theoretical point of view. For example, Wu et al. (2017) connected mean surface pressures to planar turbulent flow fields obtained from PIV measurements via the differential momentum equations, for mean flows normal to a building wall. Through this process, the effects of the upstream turbulence on the mean surface pressure distributions observed in Akon and Kopp (2016) were explained.

In general, three-dimensional and temporal flow field measurements of high resolution are required (e.g., de Kat and van Oudheusden, 2012), if the instantaneous pressure is to be evaluated theoretically. Such high costs in the flow field measurements, however, are generally not practical for typical wind engineering applications. In contrast, the quasi-steady (QS) theory, which requires less cost in measurement and calculation, offers a convenient tool in relating the wind speed and roof surface pressures. Basically, the QS method estimates the instantaneous building surface pressure using vector information of the wind measured at a point near a building. Because the analytical functions in the model are established via building surface pressure measurements, the QS approach is semi-empirical.

Because of its relative convenience, QS methods have been applied in determining the wind loads on various types of structures. For slender structures such as tall buildings (e.g., Kawai, 1983) and bridges (e.g., Davenport and King, 1984), the QS method is used to relate the local 'buffeting' velocity and wind loads on a finite section, i.e., the so-called 'strip' theory (see Holmes, 2007). For low-rise buildings, on the other hand, QS methods have been used in estimating the cladding loads, particularly on roofs, due to the significant consequences of roof failure. The simplest model accounts for only the stream-wise component of the velocity fluctuations (e.g., Uematsu and Isyumov, 1998). In addition to the streamwise component, models including the effects of transverse (e.g., Letchford et al., 1993; Richards et al., 1995) and both transverse and vertical velocities (e.g., Richards and Hoxey, 2004; Asghari Mooeneghi, et al, 2016; Wu and Kopp, 2016) have been developed as well. For turbulence with length scales larger than the building dimension, the QS method is particularly useful in relating the wind field and building surface pressures (e.g., Tieleman, 2003; Asghari Mooneghi et al., 2016; Wu, 2017).

Although QS approaches have had a somewhat successful record in wind engineering applications, the underlying physical assumptions have not been explicitly examined with respect to the Navier-Stokes equations. In order to bridge this gap, this paper links the QS vector model, of a relatively simple form, to the integral form of the momentum equations for estimations of area-averaged surface pressures. Velocity field measurements, obtained via particle image velocimetry (PIV), and point velocity measurements, via a Cobra probe, along with synchronized building surface pressures, are used for the analysis. These are described in Section 2. In Section 3, the integral momentum approach is introduced and validated for estimating area-averaged surface pressures. The QS vector model is described in Section 4. In Section 5, the physical assumptions in the QS model are explained via algebraic manipulations of the integral momentum equation. The missing terms in the QS model are further discussed and a correction is developed to account for these.

2. Experimental setup

2.1. Boundary layer flow simulations

In order to examine the effects of the upstream turbulence, the six upstream terrain conditions reported in Akon and Kopp (2016) were used to physically simulate the atmospheric boundary layer (ABL) wind. The ABL flows were generated for the experiments conducted in the high-speed section of BLTW II at UWO, which has a fetch of 39 m for flow development and cross-sectional dimensions of 3.36 m wide by 2.05 m high at the test location. Three spires that are of 1.22 m height and 0.1 m wide at the base were placed at the upstream end of the high-speed section. Using combinations of three sets of ground roughness elements (labeled as Flat, Open and Suburban) and the optional 15 inch (38 cm) barrier at the upstream end, six turbulent flow conditions (labeled as 'F0', 'F15', 'O0', 'O15', 'S0' and 'S15') were generated yielding a range of turbulence intensities (i.e., $I_u = 13\%$ to 27%) and length scales (i.e., $L_{ux} = 6H$ to $13H$). Note that the first characters in the label, i.e., 'F', 'O' and 'S', stand for 'Flat', 'Open' and 'Suburban' terrain conditions, respectively, and are a description of upstream roughness levels on the upstream tunnel floor. On the other hand, the digits '0' and '15' after the character denote heights of the upstream barrier, in inches. Table 1 summarizes the mean streamwise flow characteristics obtained from the six terrain conditions, as reported by Akon and Kopp (2016). Note that the turbulence intensity is defined as $\sqrt{\overline{u'u'}}/\overline{u}$; The integral length scale is defined as $L_{ux} = \overline{u}\int_0^\infty \overline{u'(t)u'(t+t_*)}/\overline{u'u'}\, dt_*$, where t and t_* denote time and time lag respectively; Jensen number is defined as the ratio between the building height to the aerodynamic roughness, H/z_o. As can be observed in Table 1, adding a 15-inch barrier at the upstream end significantly increases the length scale of the turbulence while increasing the roughness elements increases the turbulence intensities.

2.2. Velocity and roof surface pressure measurements on a low-rise building model

The surface pressure measurement data used in this paper were obtained on the 1/50 geometrically-scaled model of Texas Tech University Wind Engineering Research Field Laboratory (TTU WERFL) building (see Levitan and Mehta, 1992), which is shown in Figure 1 (a). The modelled building has plane dimensions of 18.3 cm × 27.5 cm with an eave height of 7.8 cm. A Cartesian coordinate used to define the space and velocity components are also included in this figure. The origin of the coordinate system is located at the middle bottom of the building model longer wall. Based on this definition, wind direction normal to the longer wall is 0° in azimuth, whereas the wind direction normal to the shorter wall is 90° in azimuth (see the definition of the wind direction azimuth in Figure 1 (a)). The upstream mean streamwise velocities are set to be around 10 m/s at model roof height for each measurement, leading to a Reynolds number of 5.3×10^4 based on the roof height. Detailed tubing system and frequency responses for the pressure measurements can be found in Ho et al. (2005). The pressures measured on this model have been studied with the velocity measurements on a planar field by Akon and Kopp (2016) and point velocity measurements by Wu and Kopp (2016) for understanding the effects of upstream turbulence. Both of the field and point velocity measurements are used in current paper and briefly summarized as follows.

The planar velocity field measurements using the time-resolved particle image velocimetry (TR-PIV) were conducted by Akon and Kopp (2016) for studying turbulent flow field near the roof. Instantaneous image pairs of particles with a time-delay of 85 micro-seconds were

captured by two 1Mb Photron FASTCAM-1024 PCI CMOS cameras. These images were transformed to the velocity data via an FFT cross-correlation algorithm in TSI Insight 4G. During the process, an interrogation window of 32×32 pixels with 50% overlap were implemented, leading to final grid spacing $\Delta x = \Delta z = 0.2$ cm for upstream field of view (i.e., FOV 1 in Figure 1 (a)) and $\Delta x = \Delta z = 0.18$ cm for roof field of view (i.e., FOV 2 in Figure 1 (a)). Note that standard cross-correlation algorithms yields a spatial uncertainty less than 0.1 pixels (Huang et al., 1997). These velocity fields were synchronized to the pressure measurements and sampled at 500 Hz for a duration of 160 seconds. More detailed discussion on the TR-PIV system and the synchronization of velocity and pressure measurements can be found in Taylor et al. (2010).

In order to study the roof surface pressure fluctuations on the TTU WERFL model (see Figure 1 (a)), Wu and Kopp (2016) conducted a separate set of measurement of three-dimensional velocity at a point location near building. A four-hole Cobra probe (TFI Inc., model no. 900, see TFI Inc., 2017), which is used to measure the 3D velocity, is placed at the location one building height ($H = 8$ cm) above the leading edge and on the symmetry plane dividing the long wall, as labeled by *m* in Figure 1 (a). In order to measure velocities that are representative of the roof top flow, the selection of the measurement location *m* is compromised with its minimal interference (see also Wu, 2017). Because one of the uses for this probe is to construct the quasi-steady (QS) model, the relative location of *m* with respect to the building is fixed for each mean wind azimuth direction. That is, when the building is rotated on the turntable in the wind tunnel, the location of *m* is also changed so that it remains directly above the leading edge (as shown in Figure 1 (a)). Both of the velocity and pressure measurement were sampled and synchronized at a rate of 625 Hz for a duration of 200 seconds. Such synchronized pressure and velocity measurements were conducted for mean wind azimuths ranges from $\overline{\theta} = 0^\circ$ to 90° with an increment of 5° and all six upstream terrain conditions described in Table 1.

3. Estimation of area-averaged mean pressure using an integral momentum equation

3.1. Background

The area-averaged pressure is an important quantity in wind engineering applications for determination of cladding loads on, for example, roof panels (e.g., Gavanski et al., 2013). In order to assess the area-averaged pressure from the field information of velocities above the roof, an integral momentum approach is applied by placing a control volume (CV) on top of the target surface of the roof (see Figure 1 (a)). Such an approach can be derived by starting with the equation of conservation of momentum for an instantaneous flow field (see, e.g., Wilcox, 2007), i.e.,

$$\frac{\partial}{\partial t}\iiint_{\mathrm{CV}} \mathbf{u}\, dV + \iint_{S} (\mathbf{u}\cdot\mathbf{n})\mathbf{u}\, ds = -\frac{1}{\rho}\left(\iint_{S} p\mathbf{n}\, ds + \iint_{S_1} p\mathbf{n}_1\, ds \right), \tag{1}$$

where $\mathbf{u}$ and p are the instantaneous velocity and pressure, respectively; S denotes the bounding surface of the CV excluding the roof surface for area-averaging, S_1 (see Figure 1 (a)); $\mathbf{n}$ and $\mathbf{n}_1$ denote the outward unit vector for surfaces S and S_1, respectively; ρ is the density of the air. The first term on the left-hand side of Eq. (1) is the time derivative of the volume-integrated velocity. The second term on the left is the instantaneous momentum flux out of the control volume. Because the velocity near the roof surface, i.e., S_1, is assumed to be zero, the

integration of the momentum flux is conducted only on rest of the surfaces bounding the CV, i.e., S. On the right-hand side of Eq. (1), the terms are associated with the pressures acting on the bounding surfaces, but with contributions of the roof surface separated from the others. Because the viscous stress plays a relatively minor role in high Reynolds number flows (e.g., Kurtulus et al., 2007; van Oudheusden et al., 2007), it is neglected in Eq. (1). Since the control volume encloses nothing but air, the force term vanishes in the momentum equation (1), which is different from the typical applications where solid objects are enclosed by the CV (e.g., Kurtulus et al., 2007; van Oudheusden et al., 2007).

By taking the time average of Eq. (1), the acceleration term vanishes. The time-average of the instantaneous momentum flux becomes a combination of mean and turbulence fluxes, i.e., $\overline{(\mathbf{u}\cdot\mathbf{n})\mathbf{u}} = (\overline{\mathbf{u}}\cdot\mathbf{n})\overline{\mathbf{u}} + \mathbf{n}\cdot\boldsymbol{\tau}$, where the overbars denote the time-average, $\boldsymbol{\tau}$ is the turbulence stress tensor, i.e., $\tau_{ij} = \overline{u_i' u_j'}$, and $\mathbf{n}\cdot\boldsymbol{\tau}$ is the contracted product, i.e., $n_j\overline{u_j' u_i'}$. The instantaneous pressure becomes the mean pressure after time-averaging. Eventually, the equation for estimating the mean area-averaged pressure over the roof surface can be obtained by rearranging, i.e.,

$$\frac{1}{\rho}\iint_{S_1}\overline{p}\mathbf{n}_1\,ds = -\iint_{S}(\overline{\mathbf{u}}\cdot\mathbf{n})\overline{\mathbf{u}}\,ds - \iint_{S}\mathbf{n}\cdot\boldsymbol{\tau}\,ds - \frac{1}{\rho}\iint_{S}\overline{p}\mathbf{n}\,ds \tag{2}$$

Given that the pressure coefficient, Cp, is defined as

$$Cp = \frac{p - p_\infty}{0.5\,\rho u_{\text{ref}}^2}, \tag{3}$$

the mean pressure coefficient averaged over surface, S_1, of area, A, which is denoted by $\overline{Cp}(S_1)$, can be obtained by subtracting the ambient static pressure, p_∞, from the time-averaged momentum equation (2) and dividing by $0.5u_{\text{ref}}^2$, i.e.,

$$\begin{aligned}\overline{Cp}(S_1)\mathbf{n}_1\,A &\equiv \iint_{S_1}\overline{Cp}\,\mathbf{n}_1\,ds \\ &= -2\iint_{S}\left[\left(\frac{\overline{\mathbf{u}}}{u_{\text{ref}}}\right)\cdot\mathbf{n}\right]\left(\frac{\overline{\mathbf{u}}}{u_{\text{ref}}}\right)ds - 2\iint_{S}\left(\frac{\boldsymbol{\tau}}{u_{\text{ref}}^2}\right)\cdot\mathbf{n}\,ds - \iint_{S}\overline{Cp}\,\mathbf{n}ds\end{aligned}. \tag{4}$$

Because the roof surface used here is flat, the surface integration of pressure on the left-hand side of Eq. (4) is further reduced to the product of the area-averaged value and the outward normal. Also, note that the mean velocity vector is now normalized by the reference velocity in Eq. (4) for the consistent definition of pressure coefficient. In this integral momentum approach, contributions to the mean area-averaged roof surface pressure coefficients can be categorized by the three terms on the right-hand side of Eq. (4): The first term is identified as the mean convection, the second is due to the turbulence and the third is due to the pressure.

Because the current PIV data are planar, as shown in Figure 1 (a), the ideal three-dimensional CV (as denoted by the red dashed lines in Figure 1 (a)) is reduced to the two-dimensional area (as denoted by the red solid lines in Figure 1 (a)) and, hence, the area-averaging becomes a line-averaging process. The resulting two-dimensional CV on top of the target roof surface is shown schematically in Figure 1 (b). Note that such a reduction in the CV dimensions requires that the flow quantities are symmetric across the measurement plane so that the two out-of-plane components involved in Eq. (4) cancel each other out. As will be shown in Section 3.2, this condition may be satisfied when the mean wind direction is normal to the long wall, i.e., $\overline{\theta}$=0°.

Since the roof slope is negligible, the outward normal of the bottom face of CV, i.e., face ① in Figure 1 (b), is $\mathbf{n}_1 = -\mathbf{k}$ for Eq. (4). Because the bottom CV face ① is close to the roof surface, the velocity and turbulence quantities are assumed to be zero and, hence, only the pressure term is involved in Eq. (4) for this face. Note that the resulting force obtained from integrating the mean pressure acting on face ①, as defined by the left-hand side of Eq. (4), has a direction parallel to the z-axis. For the CV boundaries normal to the free stream direction, i.e., faces ② and ④ in Figure 1 (b), the surfaces are exactly aligned with the *z*-axis and, hence, their outward normal vectors are parallel to the x-axis. As a result, the pressure along these two vertical boundaries are not involved in calculating the area-averaged pressure on face ① because of the orthogonality. For the top face ③ shown in Figure 1 (b), a portion of the streamline is selected as the upper boundary CV face in order to facilitate the calculation. In this manner, there is no mass flux across the upper boundary and, hence, the mean convection term vanishes for this face. Figure 1 (b) also summarizes the terms (in red texts) that need to be considered in the momentum equilibrium of Eq. (4) for each of the four CV boundary faces.

The integration of Eq. (4) can be calculated systematically by starting from the leading edge along the bottom CV border, progressing in a counter clockwise manner along the remaining CV boundaries (as indicated by the red arrows in Figure 1 (b)). The final form of time averaged momentum equation, as the result of reductions of Eq. (4) for the 2D CV shown in Figure 1 (b), can be shown to be

$$\begin{aligned}
&\overline{Cp}(S_1)\,A = \\
&2\left(\int_{S_2}\frac{\overline{u}}{u_{\text{ref}}}\frac{\overline{w}}{u_{\text{ref}}}ds - \int_{S_4}\frac{\overline{u}}{u_{\text{ref}}}\frac{\overline{w}}{u_{\text{ref}}}ds\right) \\
&+2\left(\int_{S_2}\frac{\overline{u'w'}}{u_{\text{ref}}^2}ds + \int_{S_3}\left(n_x\frac{\overline{u'w'}}{u_{\text{ref}}^2} + n_z\frac{\overline{w'w'}}{u_{\text{ref}}^2}\right)ds - \int_{S_4}\frac{\overline{u'w'}}{u_{\text{ref}}^2}ds\right) \\
&+\left(\int_{S_3} Cp\, n_z\, ds\right)
\end{aligned} \tag{5}$$

Note that the dimension of A is length in Eq. (5), instead of length square for the ideal calculation of Eq. (4). The S's in Eq. (5) denote the CV boundary surfaces with subscript indicating the specific face labeled in Figure 1 (b), whereas n_x and n_z denote the components of the outward normal unit vector along the x and z direction, respectively.

The contributions of mean convection and turbulence stresses to the line-averaged mean roof pressure can be directly evaluated from the measured PIV data. The contribution of pressure on the top face of the CV, however, is not explicitly measured. Fortunately, the Bernoulli equation along a streamline far away from the body can be used to relate the mean pressure at an upstream location and the mean pressure above the roof, as demonstrated by Wu et al. (2017). Once the required parameters are obtained along the CV boundaries, area-averaged pressures can be calculated for various regions by traversing the CV along the roof surface. The calculated results will be compared in Section 3.2 to the surface pressure measurement and the estimations obtained from differential momentum equation (i.e., the Navier-Stokes equation used in Wu et al., 2017). The reason for selecting the integral momentum approach is due to its explicit

relation to the QS theory, which will be addressed in Section 4. In order to further address this argument, the integral momentum approach of Eq. (4) needs to be validated first.

3.2. Results and discussion

The integral momentum approach described in Section 3.1 is applied to estimate the area-averaged mean roof surface pressure for a mean wind azimuth of 0°, i.e., a wind direction normal to the longer wall. The control volume (CV) used in the current calculation has a bottom width of $0.25H$ (or 2 cm, where $H = 8$ cm is the model building ridge height), as schematically indicated by the 2D solid red box in Figure 1. Based on the applicability of Bernoulli's estimation of mean pressure, as discussed in Wu et al. (2017), the main criteria of selecting a streamline as the top CV boundary is to avoid its passage through the region of high-turbulence-induced pressure gradients. Hence, streamlines far above the separated shear layer would be appropriate for this purpose. Here, we select the streamlines starting from the upstream point near $\{x = -1.5H; z = 1.31H\}$. The area-averaged mean pressures can be obtained once the information of velocity, pressure and turbulence have been extracted for the CV boundaries. The red lines in Figure 2 show the integral momentum results for the five non-overlapped segments covering a $1.25H$ (or 10 cm) fetch of roof surface, i.e., $\{0 \le x \le 1.25H,\ y = H\}$. The measured mean roof surface pressures, along with the results integrated from the Navier-Stokes equation (i.e., Figures 11 and 13 in Wu et al., 2017), are also included for comparison in Figure 2.

The distributions of $\overline{Cp}(S_1)$ estimated from the integral momentum equation are consistent with both the measurements and differential momentum (i.e., the Navier-Stokes equation) results for $x \ge 0.25H$, as can be observed in Figure 2 for terrains 'S0', 'S15'. For upstream terrain 'O0', the integral momentum result is consistent with differential momentum result but underestimated estimations of $|\Delta\overline{Cp}| \approx 0.1$ can be observed as compared to the measured values for $x \ge 0.25H$. For terrains 'F0', 'F15' and 'O15', the results obtained from the integral momentum are underestimated by $|\Delta\overline{Cp}| \approx 0.1$ for $x \ge 0.25H$, as compared to both the differential momentum solutions and measurements. It is noted that the uncertainty of surface pressure measurement is about $|\Delta\overline{Cp}| \approx 0.1$ (Quiroga Diaz, 2006) such that the existence of these differences is generally within the uncertainty band and the integral momentum approach of Eq. (4) is validated (in terms of the variations of the area-average mean pressures). For panels near the leading edge, i.e., $0 < x \le 0.25H$, the integral momentum approach generally underestimates the magnitudes by $|\Delta Cp| \approx 0.2$, as compared to the measured values. The differential momentum approach of Wu et al. (2017), however, provides relatively better estimates for this region. The difference between integral and differential momentum approaches implies that the treatment of zero velocity and turbulence near the lower boundary of a horizontally traversed CV at the ridge height may not be precise when the CV is above the leading-edge panel, since there is a gap of about 2 mm where turbulent flow may exist. Nevertheless, the detailed differences for treating the leading-edge panel do not alter the final conclusions derived from the current approach.

The contributions of convection, pressure, and turbulence to the area-averaged pressure estimated using the integral momentum equation are plotted in Figure 3, for all six terrain conditions. Generally, the convection term dominates the estimated $\overline{Cp}(S_1)$ values for areas near the leading edge, with highest contribution of around 60% of the total. For roof surfaces further downstream, the contributions of the pressure term increase near linearly, being up to 80% for panels within the bounds $\{H < x \le 1.25H\}$. The contributions of turbulence terms are generally

less than 5% and are found to be negative for some of the downstream locations. Note that these negative contributions of turbulence term are consistent with the pressure recovery observed along the leeward region of the separation bubbles described in the differential momentum approach of Wu et al. (2017).

4. The quasi-steady vector model

4.1. Background

A relatively simple version of quasi-steady (QS) vector model is introduced in this section to account for the effects of both the magnitude, $|\mathbf{u}|$, and azimuth, θ, of the instantaneous wind velocity vectors, where the variables are defined as

$$|\mathbf{u}|^2 = u^2 + v^2 + w^2 \quad \text{and} \quad \theta = \tan^{-1}\left(\frac{v}{u}\right). \tag{6a, b}$$

Typically, a QS model estimates the instantaneous building surface pressures by multiplying the instantaneous dynamic pressure measured at a point, *m*, i.e., $0.5\rho|\mathbf{u}_\mathrm{m}|^2$, with an instantaneous function Cp_inst. Note that Cp_inst is a non-dimensional quantity that is, in fact, equivalent to a pressure coefficient. However, Cp_inst varies according to a functional form which depends on input variables such as the instantaneous wind direction. Because the instantaneous wind azimuth is variable to be considered, it is included in the instantaneous function, i.e., $Cp_\mathrm{inst} = Cp_\mathrm{inst}(\theta)$. As a result, the QS vector model can be represented as

$$p - p_\infty = 0.5\,\rho\,|\mathbf{u}_\mathrm{m}|^2\, Cp_\mathrm{inst}(\theta), \tag{7a}$$

or alternatively, in the form of pressure coefficients, i.e.,

$$Cp = \frac{|\mathbf{u}_\mathrm{m}^2|}{u_\mathrm{ref}^2} Cp_\mathrm{inst}(\theta). \tag{7b}$$

A straightforward estimation of the instantaneous function can be obtained by taking the average of Cp_inst in Eq. (7b) under the condition of a specific wind azimuth, i.e.,

$$Cp_\mathrm{inst}(\theta) = \langle Cp_\mathrm{inst} \,|\, \theta\rangle = \frac{u_\mathrm{ref}^2}{\left\langle |\mathbf{u}_\mathrm{m}|^2 \,\middle|\, \theta \right\rangle} \langle Cp \,|\, \theta\rangle = \frac{u_\mathrm{ref}^2}{\overline{|\mathbf{u}_\mathrm{m}|^2}}\,\overline{Cp} \quad \left(\text{evaluated at} \quad \theta = \bar{\theta}\right). \tag{8}$$

Here $\left\langle |\mathbf{u}_\mathrm{m}|^2 \,\middle|\, \theta \right\rangle$ and $\langle Cp \,|\, \theta\rangle$ denote the average velocity squared and roof surface pressure, respectively, under the condition of specific wind azimuth. Because of the existence of the statistical independence between velocity magnitude and wind azimuth for an ABL turbulent wind, the conditional average of velocity squared, $\left\langle |\mathbf{u}_\mathrm{m}|^2 \,\middle|\, \theta \right\rangle$, can be replaced by the mean value $\overline{|\mathbf{u}_\mathrm{m}|^2}$ obtained from the measurement of the specific mean wind azimuth, $\bar{\theta} = \theta$. On the other hand, roof surface Cp values may be statistically dependent of θ. However, the conditional average of roof surface pressure coefficient, $\langle Cp \,|\, \theta\rangle$, is assumed to be equivalent to the mean pressure coefficient, $\overline{Cp}$, obtained from a measurement for the specific mean wind azimuth $\bar{\theta} = \theta$. This assumption is similar to those presented in earlier applications (e.g., Kawai, 1983; Letchford et al., 1993) and is easier for manipulations in later discussions.

By using Eq. (8), discrete estimations of the instantaneous function can be obtained for each mean wind azimuth and for each surface pressure tap location. Because of the periodicity of

$Cp_{\text{inst}}(\theta)$, the continuous form of the instantaneous function can be conveniently established by fitting the discrete values with a Fourier series (e.g., Richards et al., 1995), i.e.,

$$Cp_{\text{inst}}(\theta) = \sum_{k=0}^{N} a_{1k}\cos(k\theta) + a_{2k}\sin(k\theta), \tag{9}$$

where a_{1k} and a_{2k} are the k-th order coefficients to be determined while N denotes the maximum order being used. Such fitting can be done by minimizing the residual between fitted and measured values while keeping the maximum order, N, as low as possible.

Although it is applicable for pressure estimation at a single tap location, the QS model has been found to perform better for area-averaged pressures (e.g., Letchford et al., 1993). Therefore, the averaged roof surface pressures over a selected area are chosen for analysis and discussion. Acquiring the instantaneous function for the area-averaged pressure is relatively straightforward. Once the instantaneous function, $Cp_{\text{inst}}(\mathbf{x}_i)$, is established for each of the individual tap locations, $\mathbf{x}_i$, within the specified area, S_1, the corresponding instantaneous function for an area-averaged pressure, i.e., $Cp_{\text{inst}}(S_1)$, is simply the weighted average of the individual instantaneous functions, i.e., $Cp_{\text{inst}}(S_1) = \sum_i Cp_{\text{inst}}(\mathbf{x}_i)A(\mathbf{x}_i)/A$, because of the definition of area-averaging and the QS model, i.e.,

$$Cp(S_1) = \sum_i \frac{A(\mathbf{x}_i)}{A} Cp(\mathbf{x}_i) = \frac{|\mathbf{u}_{\text{m}}|^2}{u_{\text{ref}}^2} \sum_i \frac{A(\mathbf{x}_i)}{A} Cp_{\text{inst}}(\mathbf{x}_i) = \frac{|\mathbf{u}_{\text{m}}|^2}{u_{\text{ref}}^2} Cp_{\text{inst}}(S_1), \tag{10}$$

where $Cp(S_1)$ denotes the instantaneous area-averaged pressure coefficient for the total specified area, A, while $Cp(\mathbf{x}_i)$ denotes the pressure coefficient at the i-th tap location, $\mathbf{x}_i$, of the tributary area, $A(\mathbf{x}_i)$.

4.2. The model

Here, a portion of roof surface area near the leading edge of the longer wall covering a total of 9 pressure taps is selected for the following analyses regarding the QS theory. Note that the selected roof surface area is covered by the bottom surface of the three-dimensional CV shown in Figure 1 (a). Because QS models have been reported to perform better in explaining the large-scale turbulence effects (e.g., Tieleman, 2003; Asghari Mooneghi et al., 2016; Wu, 2017), only the results associated with the highest intensity and length scale of turbulence, i.e., terrain 'S15' in Table 1, are selected for the following discussion. Because of the symmetrical distribution of the pressure taps, the mean pressures measured at a point on the building within a quadrant of wind directions can be extended to the full range of wind directions (see Wu, 2017). These mean pressure coefficients are then used to obtain the discrete estimations of the instantaneous function via Eq. (8), which are further fitted using a Fourier series in Eq. (9) to generate the continuous form. Note that the mean upstream streamwise velocity at roof height is used as u_{ref} for defining the pressure coefficients (see Eq. (3)). Figure 4 shows both the discrete estimations and the resulting continuous form of the instantaneous function for the roof surface area. Note that the magnitudes of the Cp_{inst} values are the largest for wind direction near 0° and are reduced for wind directions normal to the shorter walls. It can be also found that the slightly larger magnitudes are skewed to $\theta = 30^{\circ}$ because the selected area is slightly closer to the smaller wall facing the 90° azimuth wind.

5. Explanation of the physical assumptions in the quasi-steady model using the integral momentum equations

5.1. The physical assumptions

As shown in Section 4 and Figure 4, the QS-estimation of the instantaneous roof surface pressure is essentially done by multiplying the instantaneous dynamic pressure by the mean roof surface pressure coefficient measured at an instantaneous wind azimuth angle. This statement becomes clear if the instantaneous function in Eq. (10) is replaced by the representation of the mean area-averaged pressure coefficient, as shown in Eq. (8), i.e., $Cp_{\text{inst}}(S_1,\theta) = \overline{Cp}(S_1,\theta=\overline{\theta})\cdot u_{\text{ref}}^2/\overline{|\mathbf{u}_{\text{m}}|^2}$, so that Eq. (10) becomes

$$Cp(S_1,\theta) = \frac{|\mathbf{u}_{\text{m}}|^2}{u_{\text{ref}}^2}\cdot\left[\frac{u_{\text{ref}}^2}{\overline{|\mathbf{u}_{\text{m}}|^2}}\overline{Cp}(S_1,\theta=\overline{\theta})\right] = \frac{|\mathbf{u}_{\text{m}}|^2}{\overline{|\mathbf{u}_{\text{m}}|^2}}\overline{Cp}(S_1,\theta=\overline{\theta}) \tag{11}$$

In order to understand the inherent physical assumptions in the QS-model, the mean area-averaged roof surface pressure coefficient, $\overline{Cp}(S_1,\theta=\overline{\theta})$, on the right hand side of Eq. (11) are further replaced by the integral momentum estimation shown in Eq. (4) so that Eq. (11) becomes

$$Cp(S_1,\theta=\overline{\theta}) = \left(\frac{|\mathbf{u}_{\text{m}}|^2}{\overline{|\mathbf{u}_{\text{m}}|^2}}\right)\left(\frac{\mathbf{n}_1}{A}\right)\cdot\underbrace{\left[-2\iint_S\left[\left(\frac{\overline{\mathbf{u}}}{u_{\text{ref}}}\cdot\mathbf{n}\right)\right]\left(\frac{\overline{\mathbf{u}}}{u_{\text{ref}}}\right)ds - 2\iint_S\mathbf{n}\cdot\left(\frac{\boldsymbol{\tau}}{u_{\text{ref}}^2}\right)ds - \iint_S\overline{Cp}\;\mathbf{n}\;ds\right]}_{\text{For flow field measured at }\overline{\theta}} \tag{12}$$

Note that the integral momentum approach in Eq. (12) implies placing a 3D CV on top of the selected roof area (see the dashed box in Figure 1 (a)) with upper boundary CV face defined by the stream surface (i.e. a collection of the streamlines) passing through the velocity measurement point, *m*. The use of this 3D CV is to explain the conceptual ideas for the following discussions instead of direct evaluation of Eq. (12). Also recall that the integral momentum approach used here is already validated in Section 3.2 for the 2D flow scenario.

By distributing the instantaneous velocity ratio, $|\mathbf{u}_{\text{m}}|^2/\overline{|\mathbf{u}_{\text{m}}|^2}$, into each part of the convection term in Eq. (12), i.e.,

$$-2\frac{|\mathbf{u}_{\text{m}}|^2}{\overline{|\mathbf{u}_{\text{m}}|^2}}\left(\frac{\mathbf{n}_1}{A}\right)\cdot\iint_S\left[\left(\frac{\overline{\mathbf{u}}}{u_{\text{ref}}}\right)\cdot\mathbf{n}\right]\left(\frac{\overline{\mathbf{u}}}{u_{\text{ref}}}\right)ds$$

$$= -2\left(\frac{\mathbf{n}_1}{A}\right)\cdot\iint_S\left[\left(\frac{|\mathbf{u}_{\text{m}}|}{\sqrt{\overline{|\mathbf{u}_{\text{m}}|^2}}}\frac{\overline{\mathbf{u}}}{u_{\text{ref}}}\right)\cdot\mathbf{n}\right]\left(\frac{|\mathbf{u}_{\text{m}}|}{\sqrt{\overline{|\mathbf{u}_{\text{m}}|^2}}}\frac{\overline{\mathbf{u}}}{u_{\text{ref}}}\right)ds\,, \tag{13a}$$

(for $\overline{\mathbf{u}}$ measured at $\overline{\theta}$)

and comparing it to the convection term of Eq. (4), it becomes clear that the QS approach assumes two physical scenarios for this term:

(i) The streamlines of the instantaneous flow field (i.e., the lines parallel to the instantaneous flow directions) near the roof are assumed to be the same as the streamlines of the mean flow field measured at the mean wind azimuth of the same value, i.e., $\overline{\theta}=\theta$. Note that a reference location such as *m* in Figure 1 (a) is used to measure the instantaneous wind azimuth, θ.

(ii) The magnitude of the instantaneous velocity is obtained by amplifying the corresponding mean velocity with an uniform rate, $\left|\mathbf{u}_{\mathrm{m}}\right| \Big/ \sqrt{\overline{\left|\mathbf{u}_{\mathrm{m}}\right|^2}}$, throughout the field. In other words, the gust is uniform and of large size (with respect to the building).

For the pressure term in Eq. (12), the goal now is to see if the two assumptions stated for the convection term are further applicable. As discussed in Section 3.1, only the pressure on the upper CV boundary face is required for evaluating the area-averaged mean surface pressure of the (horizontal) roof area (i.e., the bottom face of the 3D CV shown in Figure 1 (a)). Recall that the Bernoulli's equation can be used for calculating the mean pressure coefficient on the upper CV boundary far away from the building (see Wu et al., 2017) since the upper boundary follows a streamline, i.e.,

$$\overline{Cp}_{\mathrm{CV\,top}} = \overline{Cp}_{\mathrm{upstream}} + \frac{\left|\overline{\mathbf{u}}_{\mathrm{upstream}}\right|^2}{u_{\mathrm{ref}}^2} - \frac{\left|\overline{\mathbf{u}}_{\mathrm{CV\,top}}\right|^2}{u_{\mathrm{ref}}^2} \quad (\text{for } \overline{\mathbf{u}} \text{ measured at } \overline{\theta}),$$

where $\overline{Cp}_{\mathrm{upstream}}$ and $\overline{\mathbf{u}}_{\mathrm{upstream}}$ denote, respectively, the mean pressure coefficient and mean velocity on a streamline location far upstream of the building while $\overline{Cp}_{\mathrm{CV\,top}}$ and $\overline{\mathbf{u}}_{\mathrm{CV\,top}}$ are the corresponding quantities on a location of same streamline above the roof. Hence, by substituting the top CV boundary $\overline{Cp}$ in Eq. (12) by the Bernoulli's equation and assuming that the upstream pressure is unaffected by the building and equal to the ambient value, i.e., $\overline{Cp}_{\mathrm{upstream}} = 0$, the pressure contribution in Eq. (12) becomes

$$-\left(\frac{\left|\mathbf{u}_{\mathrm{m}}\right|^2}{\overline{\left|\mathbf{u}_{\mathrm{m}}\right|^2}}\right)\left(\frac{\mathbf{n}_1}{A}\right)\cdot \iint_{S_{\mathrm{CV\,top}}} \overline{Cp}\,\mathbf{n}\,ds$$

$$= -\left(\frac{\mathbf{n}_1}{A}\right)\cdot \iint_{S_{\mathrm{CV\,top}}} \left[\left(\frac{\left|\mathbf{u}_{\mathrm{m}}\right|}{\sqrt{\overline{\left|\mathbf{u}_{\mathrm{m}}\right|^2}}}\frac{\left|\overline{\mathbf{u}}_{\mathrm{upstream}}\right|}{u_{\mathrm{ref}}}\right)^2 - \left(\frac{\left|\mathbf{u}_{\mathrm{m}}\right|}{\sqrt{\overline{\left|\mathbf{u}_{\mathrm{m}}\right|^2}}}\frac{\left|\overline{\mathbf{u}}_{\mathrm{CV\,Top}}\right|}{u_{\mathrm{ref}}}\right)^2\right]\mathbf{n}\,ds\,. \tag{13b}$$

(for $\overline{\mathbf{u}}$ measured at $\overline{\theta}$)

As can be clearly seen on the right-hand side of Eq. (13b), the two physical assumptions of the QS model stated for the convection term are also valid for the pressure term.

Similar QS assumptions can be found for the turbulence contribution by again distributing the velocity ratio in Eq. (12) into each component of the turbulence stress tensor, i.e.,

$$-2\left(\frac{\left|\mathbf{u}_{\mathrm{m}}\right|^2}{\overline{\left|\mathbf{u}_{\mathrm{m}}\right|^2}}\right)\left(\frac{\mathbf{n}_1}{A}\right)\cdot \iint_{S} \mathbf{n}\cdot\left(\frac{\boldsymbol{\tau}}{u_{\mathrm{ref}}^2}\right) ds$$

$$= -2\left(\frac{\mathbf{n}_1}{A}\right)\cdot \iint_{S} \mathbf{n}\cdot\overline{\left(\frac{\left|\mathbf{u}_{\mathrm{m}}\right|}{\sqrt{\overline{\left|\mathbf{u}_{\mathrm{m}}\right|^2}}}\frac{u_i'}{u_{\mathrm{ref}}}\right)\left(\frac{\left|\mathbf{u}_{\mathrm{m}}\right|}{\sqrt{\overline{\left|\mathbf{u}_{\mathrm{m}}\right|^2}}}\frac{u_j'}{u_{\mathrm{ref}}}\right)} ds\,. \tag{13c}$$

(For $\overline{u_i' u_j'}$ measured at $\overline{\theta}$)

Note that because the turbulence contribution may not be as significant as the convection or pressure terms, as already shown in Figure 3 for the 2D separated-reattached flow scenario, the

amplification of the turbulence term in QS theory is expected to give relatively minor contribution as well.

In order to illustrate the two physical assumptions of the QS model, imagine two snapshots of the 3D flow fields near the roof are taken at instants t_1 and t_2, in which the instantaneous azimuths of the velocity vector measured at location *m* (Figure 1 (a)) are $\theta(t_1) = 0^\circ$ and $\theta(t_2) = -30^\circ$. For the unknown 3D flow field near the roof, the QS model assumes that the instantaneous streamlines are equivalent to the mean streamlines such that the assumed flow produces a consistent wind direction at location *m*. This is the first assumption. Therefore, for time t_1 the instantaneous flow pattern is assumed to be identical to the mean separated-reattached type of flow, as that measured at $\overline{\theta} = \theta(t_1) = 0^\circ$ (see Figure 5 (a)). Similarly, the instantaneous flow at time t_2 is assumed to be the mean conical-vortex type of pattern, exactly the same as that measured at $\overline{\theta} = \theta(t_2) = -30^\circ$ (see Figure 5 (b)).

Although the instantaneous flow direction is assumed to be identical to the mean, it is not necessarily the case for the instantaneous magnitude of the velocities. In the QS model, the instantaneous magnitudes of the velocities are assumed to be the amplified version of the mean velocity magnitude with a spatially uniform rate determined by the instantaneous velocity ratio measured at location *m*, i.e., $|\mathbf{u}_m| \Big/ \sqrt{\overline{|\mathbf{u}_m|^2}}$. Hence, for time t_1 the instantaneous flow field is assumed to be the same as the mean separated-reattached flow shown in Figure 5 (a) but with mean velocity magnitudes amplified by a rate, $|\mathbf{u}_m|(t_1) \Big/ \sqrt{\overline{|\mathbf{u}_m|^2}}$. Similarly, the velocity magnitudes of mean conical-vortex flow shown in Figure 5 (b) are amplified by a rate of $|\mathbf{u}_m|(t_2) \Big/ \sqrt{\overline{|\mathbf{u}_m|^2}}$ for constructing the instantaneous flow field at time, t_2.

5.2. Missing mechanisms in the QS model

Since the QS model is usually established on the velocity measurements at a point such as *m* in Figure 1 (a), it is impossible to accurately capture the detailed volumetric flow field required for direct evaluation of instantaneous momentum equation. However, the missing physical considerations, may be identified by comparing the QS assumptions of Eq. (12) to the exact instantaneous integral momentum equation:

$$Cp(S_1) = \left(\frac{\mathbf{n}_1}{A}\right) \cdot \left[\underbrace{-\frac{2}{u_{\text{ref}}} \frac{\partial}{\partial t} \iiint_{\text{CV}} \left(\frac{\mathbf{u}}{u_{\text{ref}}}\right) dV}_{\text{Acceleration term}} \underbrace{- 2 \iint_S \left[\left(\frac{\mathbf{u}}{u_{\text{ref}}}\right) \cdot \mathbf{n}\right] \left(\frac{\mathbf{u}}{u_{\text{ref}}}\right) ds}_{\text{Covection (\& Turbulence) term}} \underbrace{- \iint_S Cp\ \mathbf{n}\ ds}_{\text{Pressure term}} \right] \tag{14}$$

In order to make the QS assumptions for the convection and pressure terms as close as possible to the real scenarios of an instantaneous flow field, local deviations of the instantaneous flow pattern from the mean flow pattern must be minimized and the amplification rate, $|\mathbf{u}_m| \Big/ \sqrt{\overline{|\mathbf{u}_m|^2}}$, measured at location *m*, needs to be representative for the region near the roof. This requirement may be better achieved if the QS model is applied in the ABL flow of large turbulence length scale, e.g., the upstream flow cases generated with 15" barrier (see Table 1).

For point velocities measured using an instrument like a Cobra probe (TFI Inc., 2017), the instantaneous static pressure can be directly measured at point m. This information may be used to approximate the instantaneous pressure on the upper CV boundary instead of using the QS assumption in Eq. (12). In order to apply such a correction, the QS assumption for the pressure contribution is re-written using the mean static pressure coefficient measured at point m, $\overline{Cp}_{\mathrm{m}}$, i.e.,

$$-\left(\frac{\left|\overline{\mathbf{u}_{\mathrm{m}}}\right|^2}{\left|\mathbf{u}_{\mathrm{m}}\right|^2}\right)\left(\frac{\mathbf{n}_1}{A}\right)\cdot\iint_{S_{\mathrm{CV\,top}}}\overline{Cp}\;\mathbf{n}\;ds\approx\left(\frac{\left|\overline{\mathbf{u}_{\mathrm{m}}}\right|^2}{\left|\mathbf{u}_{\mathrm{m}}\right|^2}\right)\overline{Cp}_{\mathrm{m}}\qquad\left(\text{for }\overline{Cp}_{\mathrm{m}}\text{ measured at }\overline{\theta}\right)\tag{15}$$

Then, the correction is done by removing the QS assumption in the pressure term represented in Eq. (11) and compensating with the instantaneous static pressure coefficient measured at point m, Cp_{m}. In this manner, a 'static pressure corrected' QS model can be derived from the original one in Eq. (10), i.e.,

$$Cp(S_1,\theta)=\frac{\left|\overline{\mathbf{u}_{\mathrm{m}}}\right|^2}{u_{\mathrm{ref}}^2}Cp_{\mathrm{inst}}(S_1,\theta)-\left(\frac{\left|\overline{\mathbf{u}_{\mathrm{m}}}\right|^2}{\left|\mathbf{u}_{\mathrm{m}}\right|^2}\right)\overline{Cp}_{\mathrm{m}}(\overline{\theta}=\theta)+Cp_{\mathrm{m}}\,.\tag{16}$$

The missing flow acceleration term in the QS model can also be identified by comparing Eq. (12) to Eq. (14). Note that, because the acceleration contribution is a volume integral of the velocity over the entire CV, the coherence of the flow structure needs to be high so that the flow acceleration measured at point m, $\partial\mathbf{u}_{\mathrm{m}}/\partial t$, can be used to represent the overall flow acceleration within the CV. Furthermore, because of the roof surface is (near) horizontal (see Figure 1), only the acceleration of vertical velocity component plays a role. Hence, by adding the acceleration term to the static pressure corrected QS model of Eq. (16), the modified version becomes

$$Cp(S_1,\theta)=\underbrace{\frac{\left|\overline{\mathbf{u}_{\mathrm{m}}}\right|^2}{u_{\mathrm{ref}}^2}Cp_{\mathrm{inst}}(S_1,\theta)}_{\text{Basic QS model}}\underbrace{-\left(\frac{\left|\overline{\mathbf{u}_{\mathrm{m}}}\right|^2}{\left|\mathbf{u}_{\mathrm{m}}\right|^2}\right)\overline{Cp}_{\mathrm{m}}(\overline{\theta})+Cp_{\mathrm{m}}}_{\text{Static pressure correction}}+\underbrace{\left(\frac{2}{u_{\mathrm{ref}}}\right)\left(\frac{\Delta\mathrm{V}_{\mathrm{CV}}}{A}\right)\frac{\partial}{\partial t}\left(\frac{w_{\mathrm{m}}}{u_{\mathrm{ref}}}\right)}_{\text{Vertical velocity acceleration}}\tag{17}$$

where the last term on the right hand side adds the contribution of vertical velocity acceleration measured at point m and $\Delta\mathrm{V}_{\mathrm{CV}}$ denotes the volume of the CV.

5.3. Application of the QS models

In this section, the use of QS-model (denoted as 'QS-θ') established in Section 4 for prediction of the area-averaged roof surface pressure fluctuation is demonstrated for the ABL turbulent flow generated by the 'S15' terrain condition (see Table 1). The concept of the static pressure corrected QS model of Eq. (16) (denoted as 'QS-θ-p') and the further acceleration-corrected version of Eq. (17) (denoted as 'QS-θ-p-a') are also included for discussion. The comparison is done for measurements of mean wind azimuths $\overline{\theta}=0^{\circ},30^{\circ},60^{\circ}$ and 90°. The estimated time series of instantaneous $Cp(S_1)$ are compared to the measurements via the spectra ratio, coherence and probability density function (PDF). Note that the selected roof surface area, S_1, is covered by the bottom surface of the three-dimensional CV shown in Figure 1 (a), which also covers the 9 pressure taps near the leading edge of the longer wall, as indicated in Section 4.2. The spectra ratio is used to compare the magnitudes of the predicted and measured fluctuations of $Cp(S_1)$ in the frequency domain and is defined as the ratio of the spectra of the

QS-estimated $Cp(S_1)$, $S_{\mathrm{CpQS}}(n)$, to the spectra of measured $Cp(S_1)$, $S_{\mathrm{CpM}}(n)$, at frequency n, i.e.,

$$\text{Spectra ratio} = \frac{S_{\mathrm{CpQS}}(n)}{S_{\mathrm{CpM}}(n)}. \tag{18}$$

The coherence is used to evaluate the correlation between the predicted and measured $Cp(S_1)$ in the frequency domain and is defined as the real part of the normalized cross spectra between QS-estimation and measurement, i.e.,

$$\text{Coherence} = \frac{\mathrm{Re}\left[S_{\mathrm{CpQS,\,CpM}}(n)\right]}{\sqrt{S_{\mathrm{CpQS}}(n)}\sqrt{S_{\mathrm{CpM}}(n)}}, \tag{19}$$

where $\mathrm{Re}[S_{\mathrm{CpQS,CpM}}(n)]$ is the real part of cross spectra between the QS-estimation and measurements.

For mean wind azimuths of 0˚ and 30˚, near unity spectra ratio and high coherence (between 0.8 and 0.9) can be found respectively, in Figures 6 and 7, for the large length scale fluctuations i.e., $\overline{u}_{\mathrm{ref}}/n \gtrsim 10H$. This validates the QS-$\theta$ estimation of fluctuating $Cp(S_1)$ due to large length scale turbulence. On the other hand, some under- and over-estimated spectra ratios (Figure 6), and near zero coherence (Figure 7), indicate poor QS-θ-predicted fluctuating $Cp(S_1)$ due to the small length scale turbulence, i.e., $\overline{u}_{\mathrm{ref}}/n \lesssim 10H$. However, because the spectra of $Cp(S_1)$ is relatively small for the small length scale fluctuations and is monotonically decreasing with decreasing length scales, the overall effect of the small length scale fluctuations is limited such that the overall QS-θ-estimated PDFs of $Cp(S_1)$, shown in Figure 8, match well to the measurements (for $\overline{\theta}$ = 0˚ and 30˚). For mean wind azimuth of $\overline{\theta} = 60^{\circ}$, both the spectra ratio and coherence are slightly reduced for large length scale ($\overline{u}_{\mathrm{ref}}/n \gtrsim 10H$) as compared to cases of $\overline{\theta} = 0^{\circ}$ and 30°, while the conclusions of QS-θ-estimation on small length scale ($\overline{u}_{\mathrm{ref}}/n \lesssim 10H$) remains the same. A slightly underestimated $Cp(S_1)$ obtained from QS-θ model can be found in the tail regions of PDF in Figure 8 for $\overline{\theta}$ = 60˚. As the mean wind azimuth approaches 90˚, both the spectra ratio and coherence are further reduced for large length scale fluctuations. A significant reduction of the spectra ratio (to around 0.3) for the large length scale fluctuations leads to the apparent underestimation of QS-θ model in the tails of the PDF.

By adding the instantaneous correction of the static pressure to the original QS-θ model of Eq. (10), the application of QS-θ-p model in Eq. (16) is also included for comparison in Figures 6, 7 and 8. For mean wind azimuths of 0˚ and 30˚, observations from Figures 6 to 8 show that the performances of QS-θ-p model are near equivalent to the QS-θ model. Improved performance of using QS-θ-p model starts to appear for the case of $\overline{\theta}$ = 60˚, as slightly better matches of spectra ratio and PDF tail values can be observed. The most apparent improvement for using QS-θ-p model can be observed for mean wind azimuth of 90˚. In this case, the spectra ratio is near unity and a good match for the PDF tail values is observed for the QS-θ-p model. Significant improvement of the coherence for using QS-θ-p model can also be observed for the lower end of large-scale $Cp(S_1)$ fluctuations, i.e., $2H \leq \overline{u}_{\mathrm{ref}}/n \leq 100H$. Apparent improvement of QS-θ-p prediction may be expected for the re-attached flow region (i.e., the selected roof surface area for $\overline{\theta} = 90^{\circ}$) because the roof surface $Cp(S_1)$ is more significantly controlled by the static pressure on the upper CV boundary in this situation, as can be seen in Figure 3.

The further correction of the QS-θ-p model by adding the acceleration of vertical velocity does not improve the prediction performance for all analyzed cases. Direct use of vertical

546 acceleration measured at point m, i.e., $\partial w_{\mathrm{m}}/\partial t$ in Eq. (17), leads to unreasonably large
547 overestimation of small length scale $Cp(S_1)$ fluctuation. This poor estimation implies low
548 spatial coherence of vertical velocity field within the CV. To further examine the spatial
549 coherence of the vertical velocities, 2D time-resolved instantaneous flow field measurements
550 (see Section 2.2) may be used. However, because it is impossible to fully resolve the spatial
551 coherence of the velocity field using a point velocity instrument, the vertical acceleration
552 corrected QS model of Eq. (17) is not practical with the current QS method. It remains to be
553 seen if it is improved in other situations.

554 **6. Conclusions**

555 The main goal of this paper is to derive the physical assumptions embedded in the QS model
556 and investigate possible corrections based on these observations. The main findings are
557 summarized as follows:

558 • A time-averaged integral momentum approach is proposed to relate the mean flow and
559 turbulence fields to the mean area-averaged roof surface pressures. This is done by placing a
560 control volume (CV) directly above the roof panel, where the mean area-averaged pressure is
561 to be calculated. This approach is validated by the good agreement with the measured
562 values.

563 • From the time-averaged perspective, the convection term (i.e., the net momentum flux
564 through the CV) dominates the area-averaged pressures for panels beneath the separated
565 flows. For panels under the reattached flows, the static pressure just above the roof
566 dominates the mean surface pressures.

567 • A simple QS model is established to estimate the instantaneous area-averaged roof surface
568 pressures. This model accounts for the variation of magnitudes and wind azimuth measured
569 at the reference location, i.e., one building height above the leading edge.

570 • The physical assumptions embedded in the QS model are explained from simple algebraic
571 manipulations of the time-averaged integral momentum equation. Two main finding are
572 revealed:

573 o The streamlines of the instantaneous flow field must be assumed to be the same as the
574 streamlines of the mean flow field. In such a way, the assumed flow produces a
575 consistent azimuth angle of the instantaneous velocity measured at the reference location.

576 o The magnitude of the instantaneous velocity field is obtained by amplifying the mean
577 velocity field with a spatially uniform rate, $\left|\mathbf{u}_{\mathrm{m}}\right| \Big/ \sqrt{\overline{\left|\mathbf{u}_{\mathrm{m}}\right|^2}}$, where $\mathbf{u}_{\mathrm{m}}$ is the velocity vector
578 measured at the reference location.

579 • By further comparing the QS assumptions to the instantaneous integral momentum equation,
580 missing terms in the QS-model can be identified:

581 o For the QS assumption to be accurate, the instantaneous streamlines must match the mean
582 streamlines for the flow field near the roof. This ideal scenario may be better
583 approximated if the gusts have a very large scale.

584 o By using an instrument like a Cobra probe, the instantaneous static pressure can be
585 directly measured at a point location. Such information may be used to correct the QS
586 assumptions associated with the static pressure above the roof. The pressure-corrected
587 QS model is found to work better for the region of flow re-attachment. However, for a
588 roof region under flow separation, little improvement can be found by using the pressure-

corrected QS model. This is due to the fact that the static pressure on top of the roof dominates the roof surface pressure for the flow following the re-attachment point, while momentum flux contributes more for the flow separation region.

- A missing acceleration term of vertical velocity is identified in the QS assumption. However, due to limited spatial coherence of vertical velocities within the control volume (CV) outside a separation bubble on the roof, the use of the vertical velocity acceleration measured at the reference point overestimated the overall acceleration within the CV. Therefore, adding the acceleration correction to the QS model via a point velocity measurement is not suggested for practice in this particular situation.

Acknowledgement

This work was funded by the Natural Sciences and Engineering Research Council (NSERC) of Canada under the Collaborative Research and Development (CRD) program and by the Institute for Catastrophic Loss Reduction (ICLR).

References

Akon, A. F., Kopp, G. A., 2016. Mean pressure distributions and reattachment lengths for roof separation bubbles on low-rise buildings. J. Wind Eng. Ind. Aerodyn. 155, 115-125. DOI: 10.1016/j.jweia.2016.05.008

Asghari Mooneghi, M., Irwin, P., Chowdhury, A. G., 2016. Partial turbulence simulation method for predicting peak wind loads on small structures and building appurtenances. J. Wind Eng. Ind. Aerodyn. 157, 47-62. DOI: 10.1016/j.jweia.2016.08.003

Davenport, A. G., King, J. P. C., 1984. Dynamic wind forces on long span bridges. 12th IABSE congress, Vancuuver, B. C., Sep. 3-7, 1984. 705 – 712.

de Kat, R., van Oudheusden, B. W., 2012. Instantaneous plannar pressure determination from PIV in turbulent flow. Exp. Fluids 52 (2012), 1089-1106. DOI: 10.1007/s00348-011-1237-5

Gavanski, E., Kordi, B., Kopp, G. A., Vickery, P. J., 2013. Wind loads on roof sheathing of houses. J. Wind Eng. Ind. Aerodyn. 114, 106-121. DOI: 10.1016/j.jweia.2012.12.011

Ho, T.C.E., Surry, D., Morrish, D., Kopp, G.A., 2005. The UWO contributions to the NIST aerodynamic database for wind loads on low buildings: Part1. Archiving format and basic aerodynamic data. J. Wind Eng. Ind. Aerodyn. 93 (1), 1–30. DOI: 10.1016/j.jweia.2004.07.006

Holmes, J.D. 2007. Wind loading of structures. Second edition. CRC Press.

Huang, H., Dabiri, D., Gharib, M., 1997. On errors of digital particle image velocimetry. Meas. Sci. Technol. 8, 1427–1440. DOI: 10.1088/0957-0233/8/12/007

Kawai, H., 1983. Pressure fluctuations on square prisms – applicability of strip and quasi-steady theories. J. Wind Eng. Ind. Aerodyn. 13, 197–208. DOI:10.1016/0167-6105(83)90141-1

627 Kurtulus, D. F., Scarano, F., David, L., 2007. Unsteady aerodynamic forces estimation on a
628 square cylinder by TR-PIV. 42 (2), 185-196. DOI: 10.1007/s00348-006-0228-4

629 Letchford, C. W., Iverson, R. E., and McDonald, J. R., 1993. The application of the quasi-steady
630 theory to full scale measurements on the Texas Tech Building. J. Wind Eng. Ind. Aerodyn.
631 48, 111–132. DOI:10.1016/0167-6105(93)90284-U

632 Levitan, M. L., Mehta, K. C., 1992. Texas Tech field experiments for wind loads part 1:
633 building and pressure measuring system. J. Wind Eng. Ind. Aerodyn. 43 (1-3), 1565–1576.
634 DOI: 10.1016/0167-6105(92)90372-H

635 Quiroga Diaz, P.S., 2006. Uncertainty Analysis of Surface Pressure Measurements on Low-rise
636 Buildings. Master's thesis. The University of Western Ontario.

637 Richards, P.J., Hoxey, R.P., Wanigaratne, B.S., 1995. The effect of directional variations on the
638 observed mean and rms pressure coefficients. J. Wind Eng. Ind. Aerodyn. 54-55, 359-367.
639 DOI: 10.1016/0167-6105(94)00067-N

640 Richards, P. J., Hoxey, R. P., 2004. Quasi-steady theory and point pressures on a cubic building.
641 J. Wind. Eng. Ind. Aerodyn. 92, 1173-1190. DOI: doi.org/10.1016/j.jweia.2004.07.003

642 Taylor, Z. Gurka, J., R., Kopp, G.A., Liberzon, A., 2010. Long-duration time-resolved PIV to
643 study unsteady aerodynamics. IEEE Trans. Instrum. Meas., 59, 3262-3269. DOI:
644 10.1109/TIM.2010.2047149

645 Tieleman, H. W., 2003. Wind tunnel simulation of wind loading on low-rise structures: a
646 review. J. Wind Eng. Ind. Aerodyn. 91, 1627-1649. DOI: 10.1016/j.jweia.2003.09.021

647 Turbulent Flow Instrumentation (TFI), 2017.
648 https://www.turbulentflow.com.au/Products/CobraProbe/CobraProbe.php (Last date of
649 access: Dec. 28, 2017)

650 Uematsu, Y., Isyumov, N., 1998. Peak gust pressures acting on the roof and wall edges of a low-
651 rise building. J. Wind Eng. Ind. Aerodyn. 77 & 78, 217-231. DOI: 10.1016/S0167-
652 6105(98)00145-7

653 van Oudheusden, B. W., Scarano, F., Roosenboom, E. W. M., Casimiri, E. W. F., Souverein, L.
654 J., 2007. Evaluation of integral forces and pressure fields from planar velocimetry data for
655 incompressible and compressible flow. Exp. Fluids. 43, 153-162. DOI: 10.1007/s00348-
656 007-0261-y

657 Wilcox, D. C., 2007. Basic Fluid Mechanics, Third edition. DCW Industries, Inc., USA.

658 Wu, C.-H., Kopp, G. A., 2016. Estimation of wind-induced pressures on a low-rise building
659 using Quasi-Steady theory. Frontiers in Built Environment. 2, 5. DOI:
660 10.3389/fbuil.2016.00005
661

662 Wu, C.-H., 2017. Estimation of turbulence effects on wind-induced suctions on the roof of a
663 low-rise building. Electronic Thesis and Dissertation Repository. 4855.
664 http://ir.lib.uwo.ca/etd/4855

665 Wu, C.-H., Akon, F., Kopp, G. A., 2017. Effects of turbulence on the mean pressure field in the
666 separated-reattaching flow above a low-rise building. J. Wind Eng. Ind. Aerodyn. 171, 79-
667 92. DOI: 10.1016/j.jweia.2017.09.013.

Figures

a

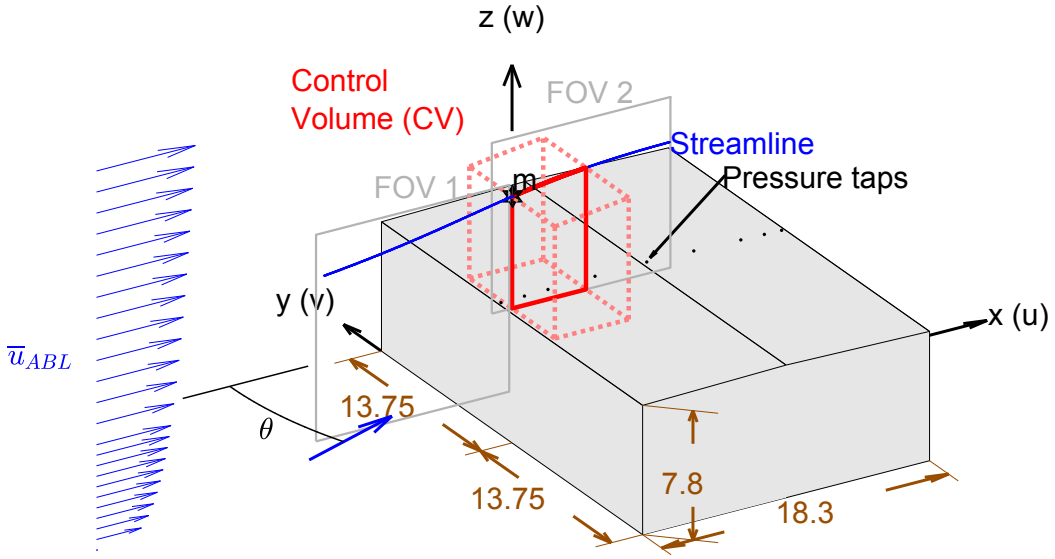

b

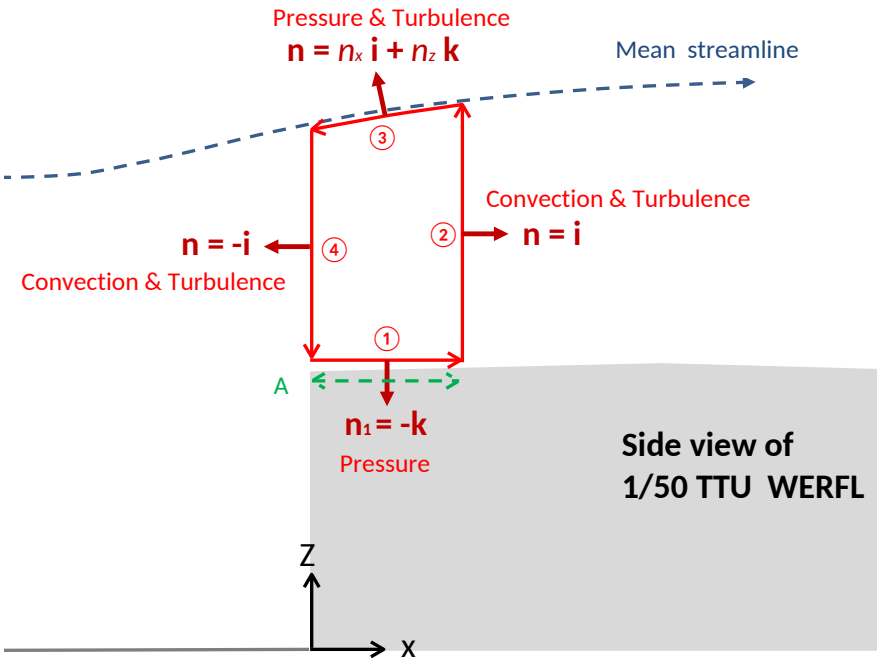

Figure 1: (a) The low-rise building model along with planar fields of view (FOV) of the PIV measurements. The dimensions of the building model are labelled with units in centimeters. A three dimensional control volume for analyses of integral momentum approach is placed on top of the roof surface where area-averaged pressures are calculated; (b) Reduced 2D control volume on top of the roof surface where line-averaged roof surface pressure is calculated.

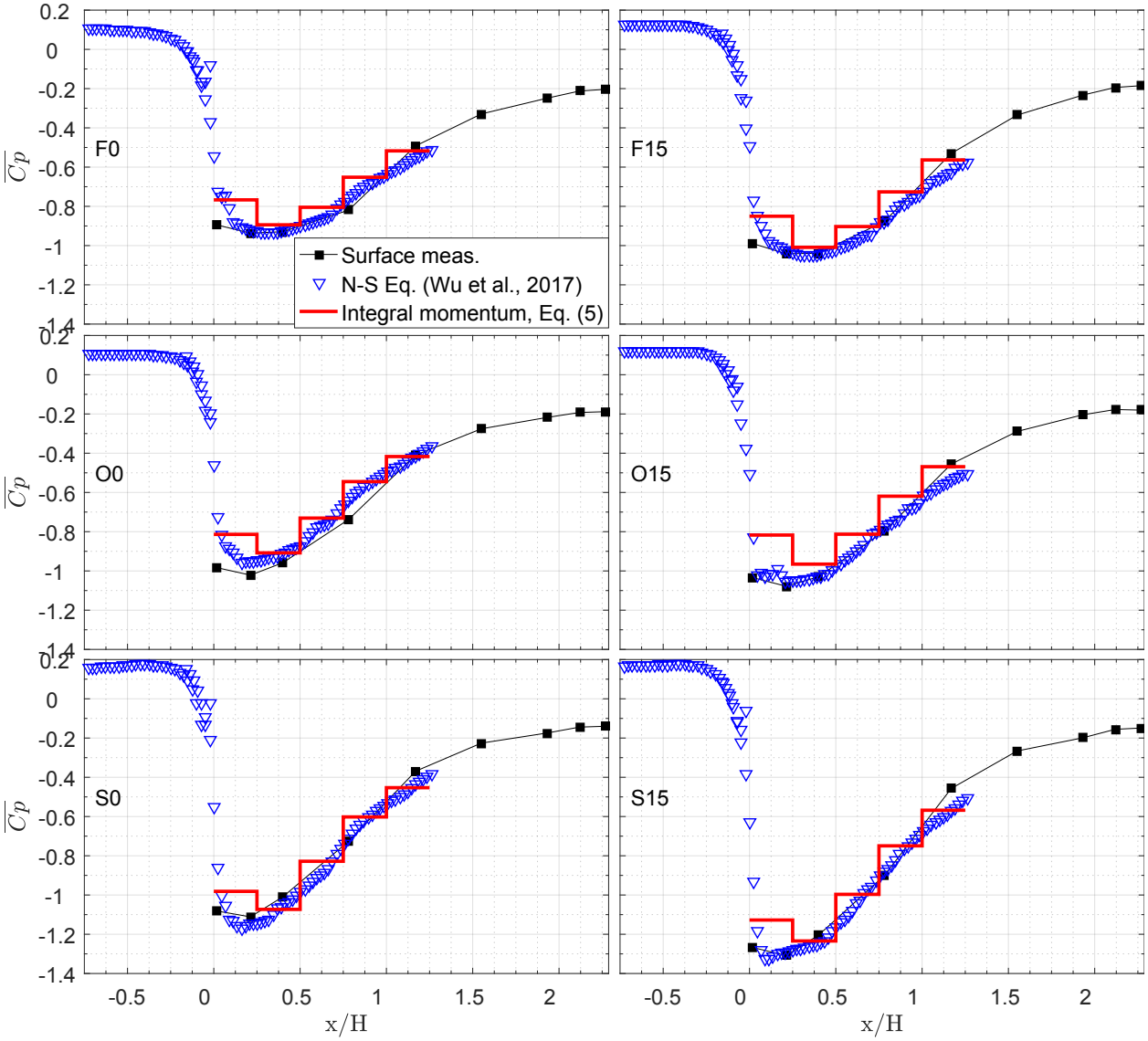

Figure 2: Surface pressure measurement and estimations obtained from integral and differential momentum equations for the six upstream terrain conditions.

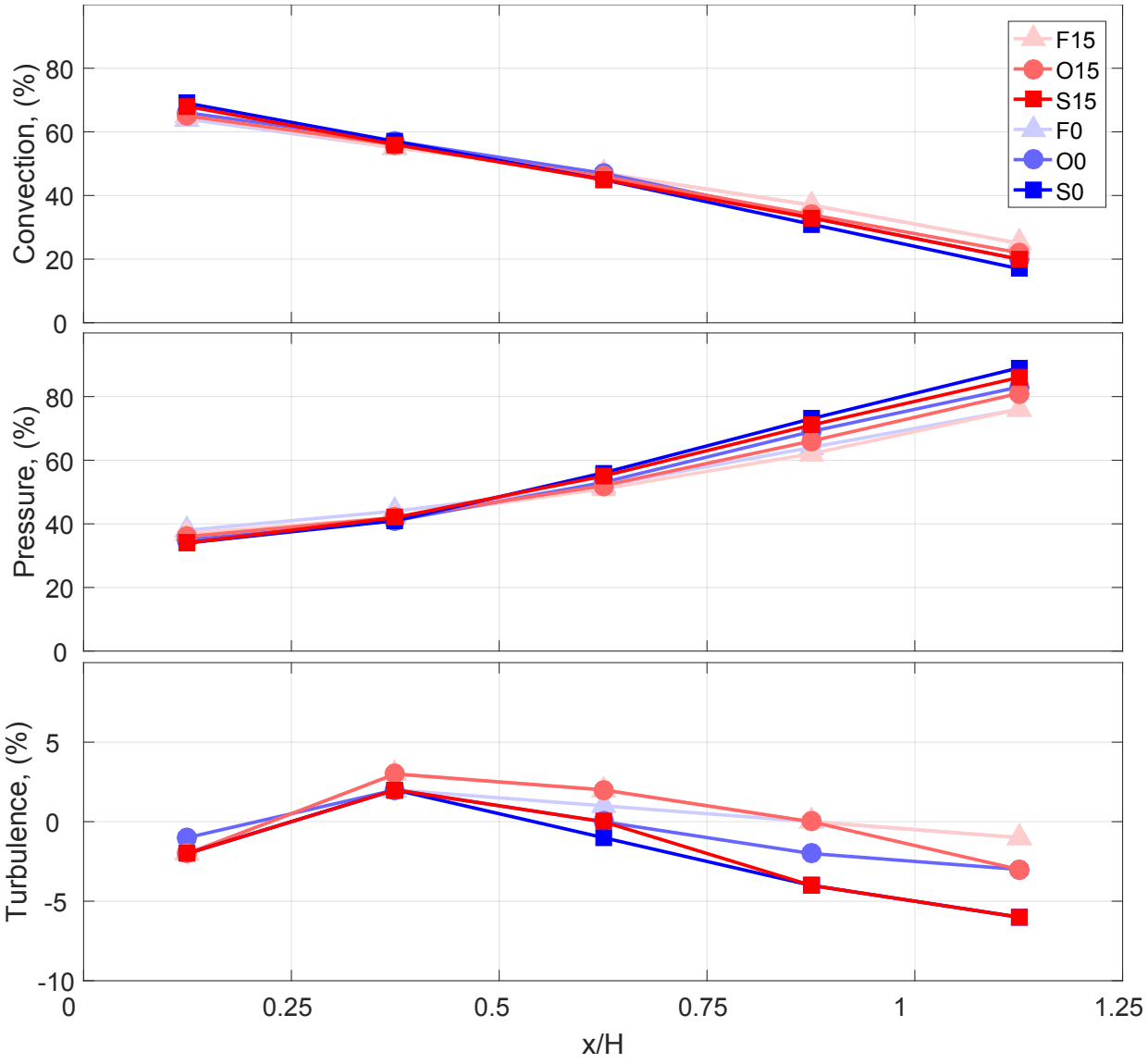

Figure 3: Contribution of convection, pressure and turbulence terms in integral momentum equation to the area-averaged mean roof surface pressure.

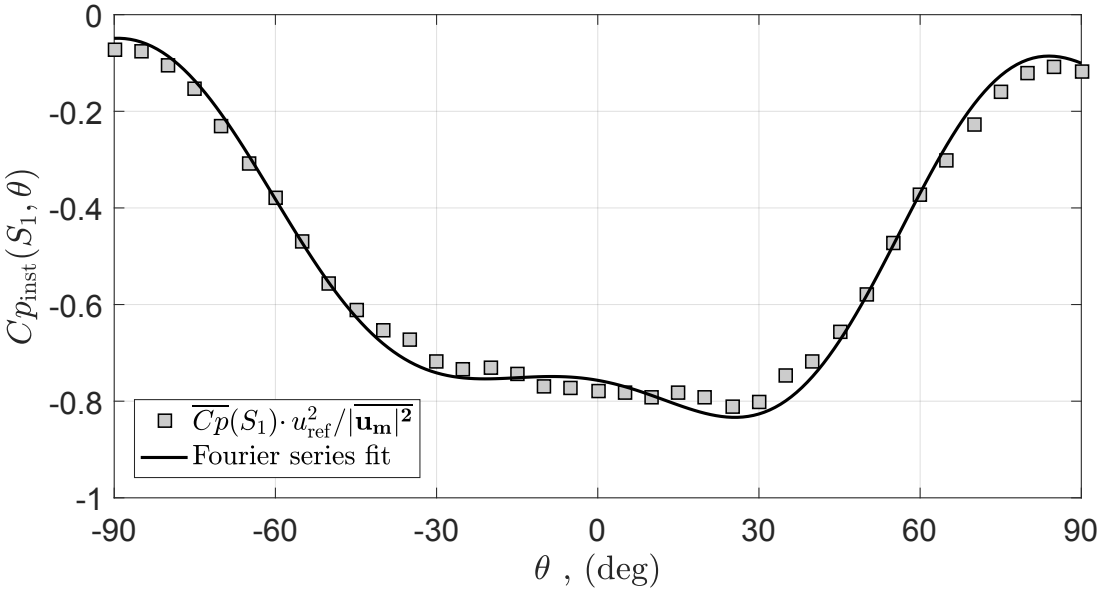

Figure 4: Fourier series fit of the instantaneous function for the selected roof surface area in terrain 'S15'.

a

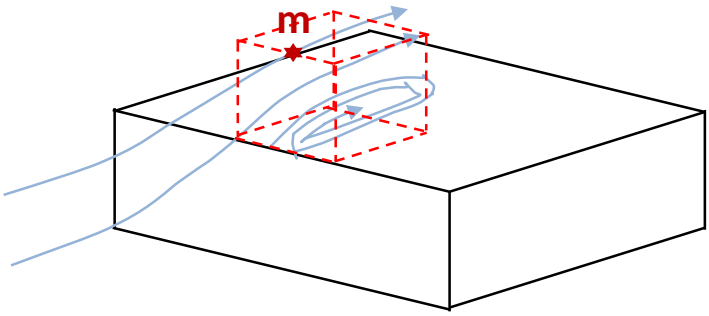

b

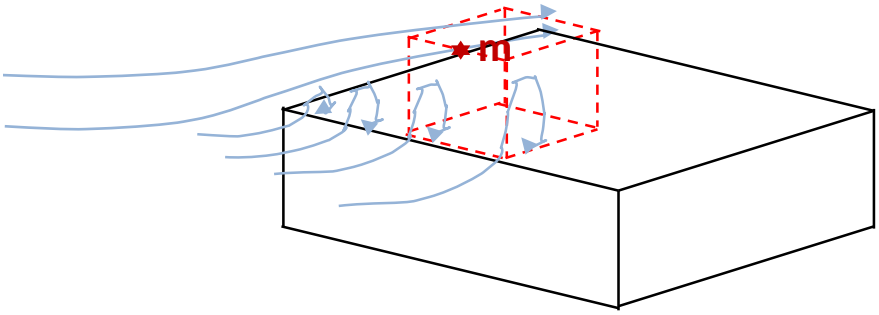

Figure 5: Schematic control volume and mean streamlines on top of the roof for mean wind azimuths: (a) $\overline{\theta} = 0^{\circ}$ and (b) $\overline{\theta} = -30^{\circ}$.

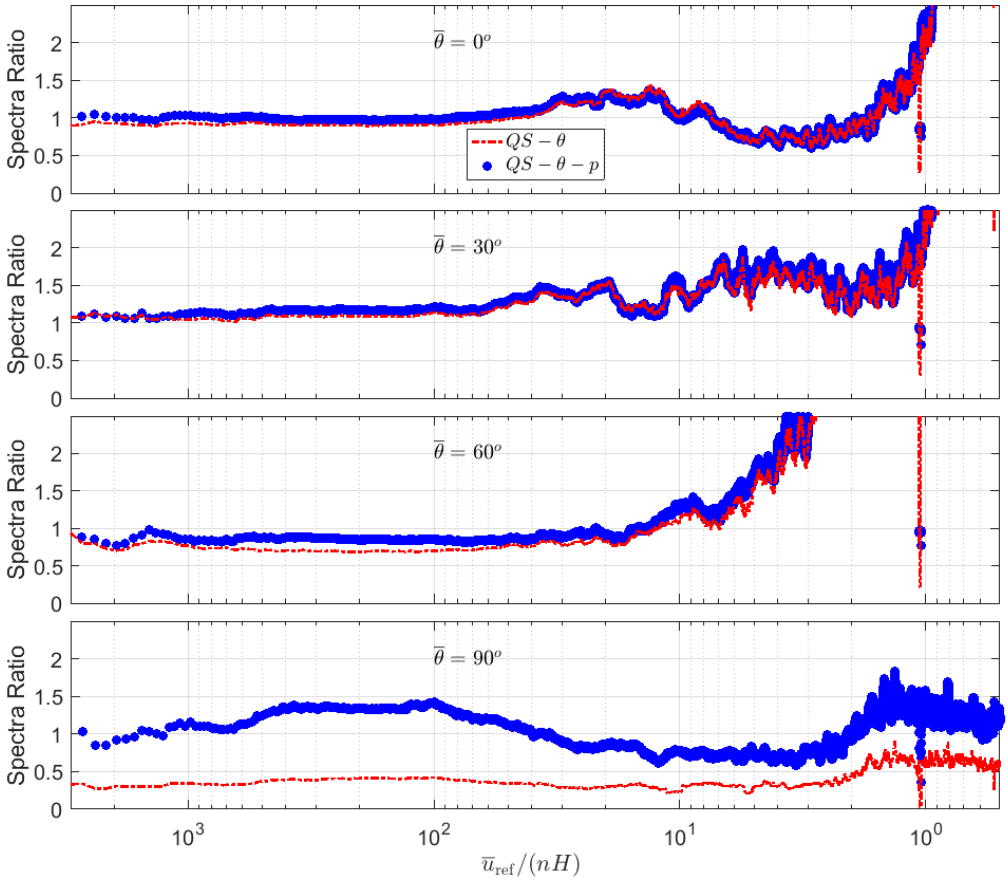

Figure 6: The ratio of QS-estimated spectra to measured spectra of $Cp(S_1)$ for various mean wind azimuths in terrain S15.

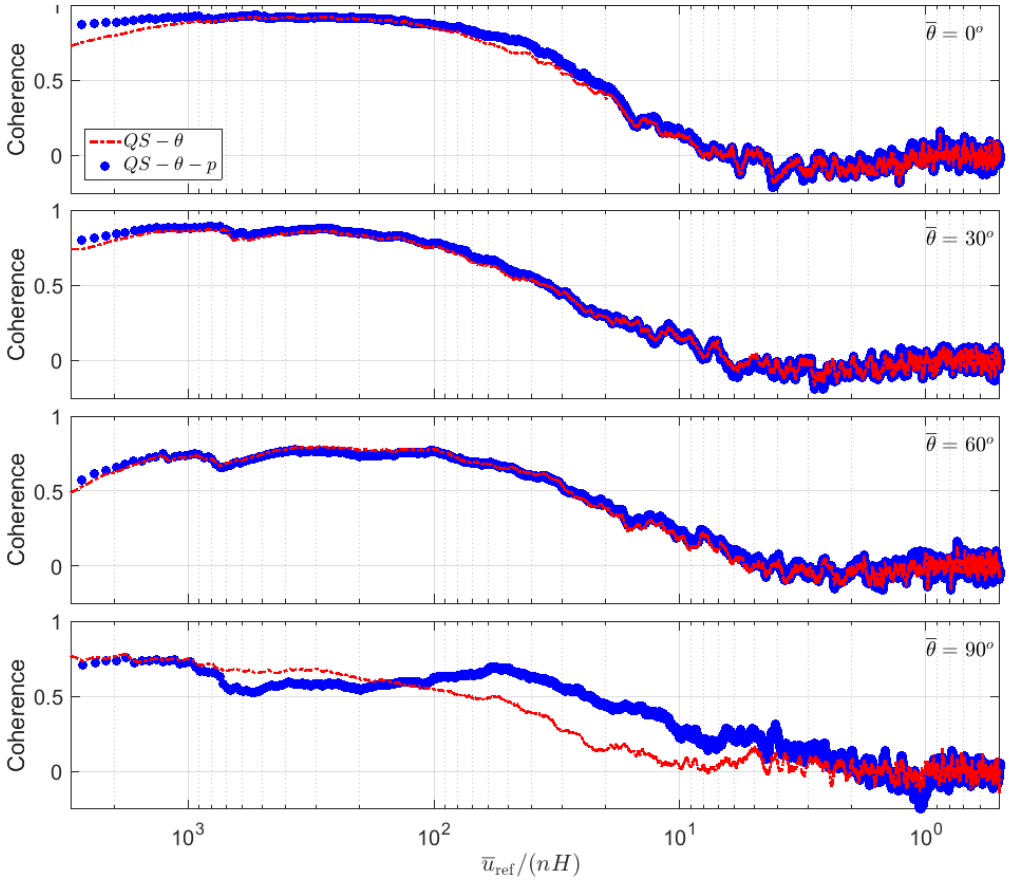

Figure 7: The coherence between QS-estimated and measured $Cp(S_1)$ for various mean wind azimuths in terrain S15.

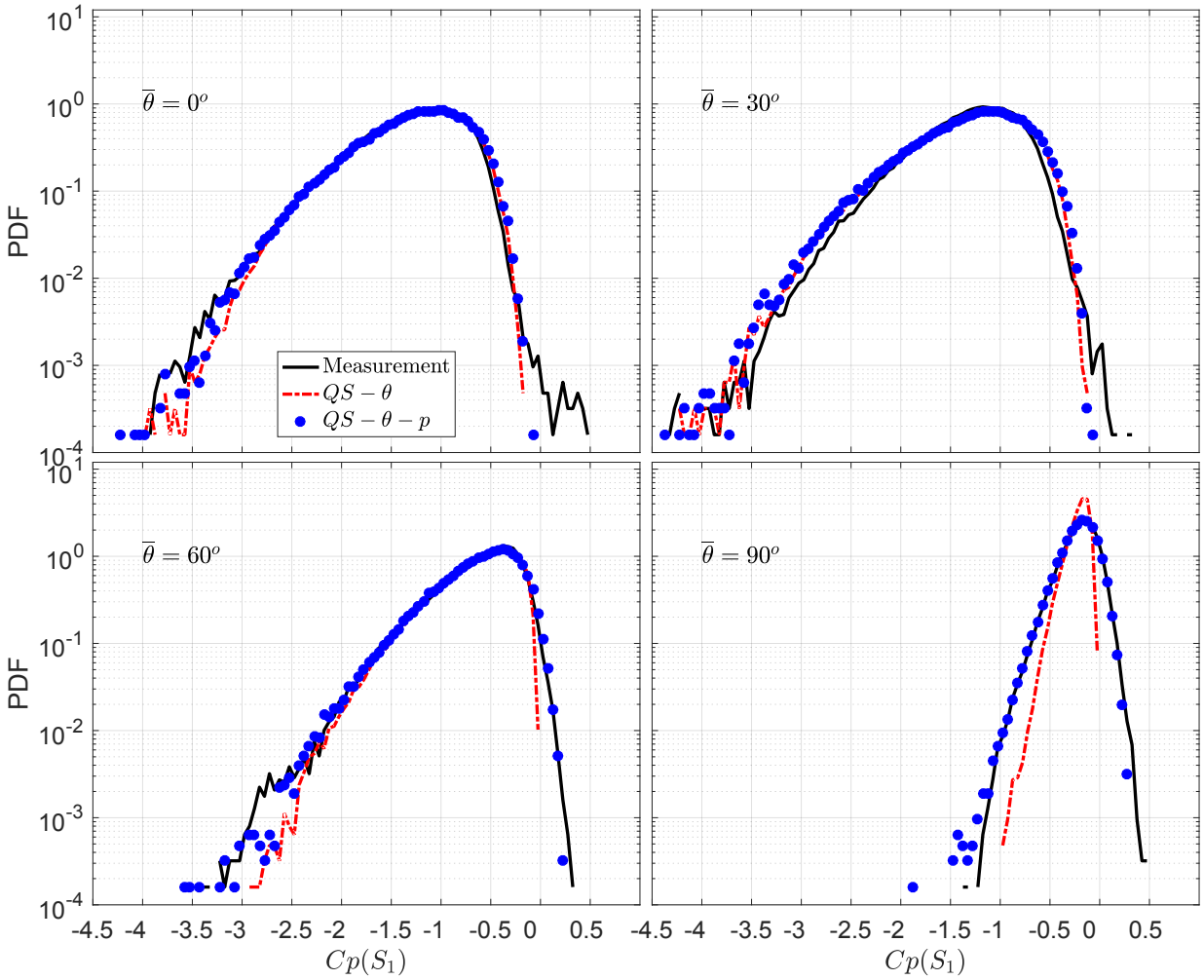

Figure 8: Probability density function (PDF) of QS-estimated and measured $Cp\left(S_1\right)$ for various mean wind azimuths in terrain S15.

Tables

Table 1: Characteristics of mean streamwise velocity and turbulence measured at model roof height (Akon and Kopp, 2016).

Ground roughness level	Flat		Open		Suburban	
Upstream barrier height	N/A	15 inch	N/A	15 inch	N/A	15 inch
Label	F0	F15	O0	O15	S0	S15
Turbulence intensity, I_u (%)	13	14	17	17	26	27
Integral length scale ratio, L_{ux}/H	6	13	8	11	7	12
Jensen number, H/z_o	540	600	290	600	56	71